

# Gain-driven singular resonances in active core-shell and nano-shell plasmonic particles

KAREN CAICEDO,<sup>1</sup> ANDRES CHATEY,<sup>2</sup> MELISSA INFUSINO,<sup>3</sup> ASHOD ARADIAN<sup>4</sup> AND ALESSANDRO VELTRI<sup>3,\*</sup>

<sup>1</sup>Univ. Bordeaux, CNRS, IOGS, LP2N, UMR 5298, F-33400 Talence, France

<sup>2</sup>Max Planck Institute for Plasma Physics, Boltzmannstr. 2, 85748 Garching, Germany

<sup>3</sup>Colegio de Ciencias e Ingeniera, Universidad San Francisco de Quito, Quito, Ecuador

<sup>4</sup>Univ. Bordeaux, CNRS, CRPP, UMR 5031, F-33600 Pessac, France, UPR 8641, F-33600 Pessac, France

\*aveltri@usfq.edu.ec

**Abstract:** Within the frame of a simple, long-wavelength, quasi-static description, we present a theoretical characterization of the optical response of metal nanoparticles doped with active gain elements in a core-shell (metallic core within an active dielectric shell) and nano-shell (active dielectric core within a metallic shell) configurations. The common feature of these structures is that, adding gain to the system produces an increase of the quality of the plasmon resonance, which becomes sharper and sharper until a singular point, after which, the system switches from absorptive to emissive (nanolaser). We use this aforementioned simple model to develop a general method allowing to calculate both the expected singular plasmon frequency and the gain level needed to realize it, and to discuss the spectral deformation occurring before and after this singular point. Finally we propose a way to calculate if the singular behavior is reachable using realistic amounts of gain.

© 2022 Optical Society of America

The last decade has seen the study of resonant plasmonic nanostructures (including noble metals and active elements), steadily gaining momentum within the field of plasmonics while attracting interest in both optoelectronics and nanotechnology due to the variety of the possible applications: nano-resonators in noble metals are, in fact, good candidates for the realization of visible-range metamaterials, where the embedding of optical gain (organic dye molecules or nanocrystals) is possibly the most promising strategy to circumvent the high level of losses they present at these frequencies [1–16], which are, just to mention an example, the primal reason for which the realization of metamaterial based cloaking devices [17–19] at visible frequencies have practically been put aside. Moreover, metallic nanostructures with gain elements are nanoscale sources of strong optical fields; this intriguing feature, culminating in the conception of the SPASER, widened their potential applicability to nanoscale lithography, probing, microscopy and more [20–23]. In the zoo of proposed nanostructures, a prominent role is played by core-shell and nano-shell nanoparticles, for they are controllable and stable plasmonic structures including all features needed for diverse optoelectronic applications [24–27], and they are obtainable in large numbers via nanochemical synthesis [28, 29].

In a previous work [30], we studied the simpler situation of a single, homogeneous metallic nanoparticle immersed in a gain medium; focusing on the plasmonic response, with its amplification and distortions. In that study we have shown that new types of responses arise as the gain level is modified and we emphasized striking differences between gold and silver nanoparticles: when silver is used, the behavior is rather straightforward, with an increasing quality of the plasmon resonance as the amount of gain elements is increased towards the singular point; in gold structures (due to the higher loss associated with the interband transition), the situation is richer, and produces increasingly distorted spectra as the gain increases culminating in the appearance of a “conjugate” plasmon which arise as a Fano-type interference between the plasmon and

46 the gain resonance curve. This new behavior shows one particularly attractive property from  
 47 the application standpoint: at the plasmon frequency, the real response is maximal, and losses  
 48 are close to zero. One of the main objectives of this work is the use of the aforementioned  
 49 approach for the description of the behaviour of systems experimentally achievable such as gain  
 50 functionalized core-shell and nano-shell nanoparticle.

51 The previous model hypothesized an infinite active media surrounding the nanoparticle,  
 52 uniform in density of molecules and pumping rate. If not completely unrealistic, this system is  
 53 experimentally unpractical to the least, especially for application requiring a single nanoparticle  
 54 and not a population. Moreover, we believe that is definitely interesting to verify if the more  
 55 appealing features of the deformed spectra survive when relaxing the infinite/uniform gain media  
 56 approximation. For these reasons, we propose here a model for gain embedded nanoparticles in  
 57 the core-shell (with metal core and a dielectric shell including gain elements) and nano-shell  
 58 (with metal shell and a dielectric core including gain elements) configurations. By introducing  
 59 the aspect ratio  $\rho$  as the ratio between the internal and the external radius of these structures and  
 60 a parameter  $G$  that will be defined later, which accounts for the quantity of gain in the system, we  
 61 will explore the  $[\rho, G]$  parameter space looking for all of the interesting behaviors discussed in  
 62 our previous work and more.

### 63 1. Core-shell and nano-shell geometries

64 We consider a single spherical nanoparticle (NP) whose core, of a relative permittivity  $\epsilon_c$ , is  
 65 defined by the inner radius  $r_1$ ; this core is covered by a coating shell of permittivity  $\epsilon_s$  located  
 66 in the space between  $r_1$  and the external radius  $r_2$  of the nanoparticle. The whole system is  
 67 immersed in a dielectric host medium with relative permittivity  $\epsilon_h$ . In the quasi-static limit,  
 68 where the size of the nanoparticle is enough smaller than the exciting wavelength, the dipolar  
 69 polarizability  $\alpha$  of such a NP is classically given as [31]:

$$\alpha(\omega) = 4\pi r_2^3 \epsilon_h \frac{(\epsilon_s - \epsilon_h)(\epsilon_c + 2\epsilon_s) + \rho^3(\epsilon_c - \epsilon_s)(\epsilon_h + 2\epsilon_s)}{(\epsilon_s + 2\epsilon_h)(\epsilon_c + 2\epsilon_s) + 2\rho^3(\epsilon_s - \epsilon_h)(\epsilon_c - \epsilon_s)} \quad \text{where } \rho = \frac{r_1}{r_2}. \quad (1)$$

70 The difference between the core-shell and the nano-shell, here resides in the definition of the  
 71 permittivities  $\epsilon_c$  and  $\epsilon_s$ : by using a metal permittivity for  $\epsilon_c$  and a gain assisted dielectric one for  
 72  $\epsilon_s$  equation 1 represent a core-shell nanoparticle, by doing the reverse it describes a nano-shell  
 73 one. The polarizability of a nanoparticle couples the total dipole moment  $\mathbf{p}$  with the local electric  
 74 field  $\mathbf{E}_{\text{loc}}$  as  $\mathbf{p} = \alpha \epsilon_0 \mathbf{E}_{\text{loc}}$  and it is related to the absorbance, the effective permittivity and all the  
 75 nano and mesoscopic electromagnetic parameters of interest. For this reason it constitutes a  
 76 reference for the most common optical characterizations.

77 In the calculations we will carry out in this article, all material permittivities will be denoted as  
 78  $\epsilon = \epsilon' + i\epsilon''$ , with  $\epsilon'$  (resp.  $\epsilon''$ ) the real (resp. imaginary) part. We follow the optics convention:  
 79 losses correspond to  $\epsilon'' > 0$ , and gain to  $\epsilon'' < 0$ .

80 The metal dielectric permittivity  $\epsilon_m$  as a function of the angular frequency  $\omega$ , is interpolated  
 81 from the Johnson & Christy dataset [32] for gold and silver, and always displays a positive  
 82 imaginary part  $\epsilon_m''(\omega)$  due to Ohmic losses.

83 The active gain medium is modeled using a single Lorentzian emission lineshape:

$$\epsilon_g(\omega) = \epsilon'_g(\omega) + i\epsilon''_g(\omega) = \epsilon_b + \frac{G\Delta}{2(\omega - \omega_g) + i\Delta}, \quad (2)$$

84 where  $\epsilon_b$  is the real, positive permittivity of the background dielectric medium embedding the  
 85 gain elements (emitters such as dye molecules, quantum dots, etc.),  $\Delta$  sets the emission bandwidth  
 86 and  $\omega_g$  is the central frequency of the emitters. These gain elements are assumed to be externally  
 87 pumped at some (absorption) frequency located sufficiently far away from the plasmon resonance.

88 The important quantity  $G$  represents the global level of gain in the amplifying medium and is  
 89 taken as a real, positive quantity. The higher the gain level in the system, the more positive the  
 90 value of  $G$  gets.

91 To provide gain and compensate for the losses in the metallic parts,  $\varepsilon_g''(\omega)$  is indeed negative,  
 92 and the maximum of emission is obtained for  $\omega = \omega_g$  with opposite sign to the parameter  $G$ :  
 93  $\varepsilon_g''(\omega_g) = -G < 0$ .

94 The gain level  $G$  is related to microscopic quantities as follows (see section 6 for details):

$$G = \frac{2\mu^2}{3\hbar\varepsilon_0\Delta}n\tilde{N} > 0, \quad (3)$$

95 where  $\mu$  is the transition dipole moment of the emitters,  $\hbar$  the reduced Plank constant,  $n$  the  
 96 volume density of gain elements, and  $\tilde{N}$  the population inversion (i. e. the pumped fraction of  
 97 the of the gain elements population). In this article, we will be considering the response of the  
 98 system to variations in the gain level  $G$ : once a specific dye is chosen (i.e.,  $\mu$  and  $\Delta$  are set), these  
 99 variations can be obtained either by changing the density of emitters  $n$  within the gain region  
 100 of the nanoparticle, or, for a given density, by modifying the pump power (which changes  $\tilde{N}$ ).  
 101 The latter is obviously more practical but gives access to a limited range of  $G$  values, since the  
 102 inversion population rapidly saturates to a maximum. Changes in the density of gain elements  
 103 allow to reach higher gain values by packing more emitters, although there are also limitations,  
 104 as discussed in section 6.

105 Equation 2 is widely used and accepted as a way to model gain media [16, 27, 33–36], but  
 106 in the context of nanolasing, it indeed represents a strong approximation: this is presupposing  
 107 that (i) the system is capable of reaching a steady state of emission; (ii) the gain medium can be  
 108 described as a homogeneous medium, with a permittivity  $\varepsilon_g$ . None of these is obvious, since  
 109 emissive states are in essence dynamical, and described *via* time and space-dependent equations  
 110 involving the population densities of various electronic levels. In a previous work [37], we studied  
 111 the emission of a nanoparticle in a infinite gain medium, using a detailed dynamical model based  
 112 on the optical Bloch equations: we found that, as long as the system remains lossy (passive)  
 113 for some frequency  $\omega$  (i.e., the imaginary part of the polarizability is positive,  $\alpha''(\omega) > 0$ ), the  
 114 steady-state description of the gain medium holds at that frequency. Where the system becomes  
 115 emissive with  $\alpha''(\omega) < 0$ , however, we found that the response in the gain medium becomes  
 116 non-linear and depends locally on the spatially-varying intensity of the electrical field, so that a  
 117 simple permittivity-based description similar to equation 2 becomes irrelevant.

118 Therefore, we emphasize strongly that in what follows, one should exercise caution in reading  
 119 charts presenting the evolution of, e.g., the polarizability versus the level of gain  $G$ : the simplified  
 120 description put forward in this article works reliably only when  $\alpha''(\omega) > 0$ , and enables us,  
 121 in particular, to calculate the response of the nanoparticle up to and at the singularity point.  
 122 Beyond the singularity point, all lasing states, where  $\alpha''(\omega) < 0$ , will not be describable using  
 123 this formalism (the corresponding areas in charts will be identified using a grey shading).

## 124 2. Singular resonance

A lot of the most exciting applications require the system to emit and while (as we just discussed)  
 the precise phenomenology of the emissive (lasing) states of the nanoparticle is outside the  
 possibilities of this model, we can still use it to calculate the threshold gain  $G_{\text{th}}$  needed for the  
 system to start emitting. In all but a few exceptional cases (see further), the switch between  
 absorption and emission behaviours happens when the denominator of equation 1 vanishes and a  
 singularity is produced. Since the denominator is different for core-shells and nano-shells, we

get two conditions:

$$(\varepsilon_m + 2\varepsilon_h)(\varepsilon_g + 2\varepsilon_m) + 2\rho^3(\varepsilon_m - \varepsilon_h)(\varepsilon_g - \varepsilon_m) = 0 \quad \text{for nano-shells,} \quad (4)$$

$$(\varepsilon_g + 2\varepsilon_h)(\varepsilon_m + 2\varepsilon_g) + 2\rho^3(\varepsilon_g - \varepsilon_h)(\varepsilon_m - \varepsilon_g) = 0 \quad \text{for core-shells;} \quad (5)$$

125 solving for  $\varepsilon_g$ , both conditions can be reduced to the form:

$$\varepsilon_g(\omega) = F(\rho, \omega), \quad (6)$$

126 where the function  $F(\rho, \omega)$  is defined as:

$$F(\rho, \omega) = \varepsilon_m \frac{2\varepsilon_m(\rho^3 - 1) - 2\varepsilon_h(\rho^3 + 2)}{\varepsilon_m(2\rho^3 + 1) + 2\varepsilon_h(1 - \rho^3)}, \quad (7)$$

for the nano-shell structures, and

$$F(\rho, \omega) = \frac{\sqrt{(\varepsilon_h - \varepsilon_m)^2[4\rho^3(\rho^3 + 1) + 1] + 3\varepsilon_h[\varepsilon_h(4\rho^3 + 5) + 2\varepsilon_m(10\rho^3 - 1)]}}{4(1 - \rho^3)} + \frac{\varepsilon_h(\rho^3 + 2) + \varepsilon_m(2\rho^3 + 1)}{4(1 - \rho^3)} \quad (8)$$

127 for the core-shell structures. Note that the function  $F$  depends only on the structural parameters  
128 of the nanoparticle (materials and aspect ratio), but not on the gain level in the system. Note  
129 also that, while equation 4 is linear in  $\varepsilon_g$ , equation 5 is quadratic: this means that a second  
130 solution (other than the one presented in equation 8) exists in principle for core-shells; however,  
131 it produces non-physical effects such as negative values for  $G_{\text{th}}$ , so that it can be safely dismissed.

132 Condition 6 not only defines the threshold gain  $G_{\text{th}}$ , i.e. the minimal gain in the system  
133 necessary to obtain a singular plasmon, it also yields the singular resonance frequency  $\omega_{\text{sp}}$ ; in  
134 both the core-shell and the nano-shell case, by substituting expression 2 in equation 6, one can  
135 easily obtain the following relation:

$$\frac{G_{\text{th}}\Delta}{4(\omega_{\text{sp}} - \omega_g)^2 + \Delta^2} = \frac{F(\rho, \omega_{\text{sp}}) - \varepsilon_b}{2(\omega_{\text{sp}} - \omega_g) - i\Delta}, \quad (9)$$

136 We note that the left-hand side of equation 9 is real, while the right-hand term is complex, so that  
137 the imaginary part of the right-hand term must be zero:

$$\Delta[F'(\rho, \omega_{\text{sp}}) - \varepsilon_b] + 2F''(\rho, \omega_{\text{sp}})(\omega_{\text{sp}} - \omega_g) = 0 \quad (10)$$

138 where  $F'$  and  $F''$  are the real and imaginary parts of  $F$ . This last equation allows to calculate  
139  $\omega_{\text{sp}}$ ; once this is known, we can use the real part of equation 9 to calculate:

$$G_{\text{th}} = \frac{2}{\Delta}(\omega_{\text{sp}} - \omega_g) [F'(\rho, \omega_{\text{sp}}) - \varepsilon_b] - F''(\rho, \omega_{\text{sp}}). \quad (11)$$

140 It should be noted that, when using expression 7 for  $F$  (nano-shell), condition 9 is the same as  
141 that derived in [38], where it was directly calculated from boundary conditions. It can be also  
142 of interest that if one uses  $F(\omega, \rho) = \varepsilon_m/2$ , the same procedure gives  $G_{\text{th}}$  and  $\omega_{\text{sp}}$  for a single  
143 metal particle in a infinite and uniform gain medium [30].

144 One can see that both  $\omega_{\text{sp}}$  and  $G_{\text{th}}$  depend on  $\rho$  and on the distance  $(\omega_{\text{sp}} - \omega_g)$  between the  
145 singular plasmon frequency and the gain center position. It is possible to show that the most  
146 effective coupling between the gain emission and the plasmon occurs when  $\omega_g = \omega_{\text{sp}}$ , i.e., when  
147 the gain emission is centered on the singular plasmon it is feeding; then, the singular plasmon is

148 obtained with the minimal global level of gain. The further apart one sets  $\omega_g$  from  $\omega_{sp}$ , the less  
 149 effective is the coupling (i.e., the value of  $G_{th}$  increases). In the following, we will assume that  
 150 the gain positioning is always optimal with respect to the resonance ( $\omega_g = \omega_{sp}$ ), including when  
 151 the value of  $\rho$  is changed (in the nano-shell geometry, this leads to a shift of  $\omega_{sp}$ , and therefore  
 152  $\omega_g$  has to be adjusted accordingly to follow). We stress that this is not a physical prerequisite, but  
 153 it will make the following discussion much simpler.

Under such optimal gain positioning, equations 10 and 11 simplify into:

$$F'(\rho, \omega_{sp}) = \varepsilon_b \quad (12)$$

$$G_{th} = -F''(\rho, \omega_{sp}), \quad (13)$$

154 this way making  $\omega_{sp}$  and  $G_{th}$  functions of  $\rho$  only.

155 One final important remark is in order: even in the quasi-static, dipolar regime under  
 156 consideration, these nanoparticles may in principle support more than one resonance (i. e.,  
 157 there may be several solutions for  $\omega_{sp}$  in equation 10). This is especially true for the nano-shell  
 158 geometry, which is known for supporting symmetric and antisymmetric modes [39]. In the  
 159 following, we always chose to focus on the most intense resonance only, which is the one requiring  
 160 the lowest amount of gain to reach singularity and be driven to emission: this is the most relevant  
 161 situation to consider for the means of practical feasibility of a plasmonic nanolaser. (In the case  
 162 of a nano-shell system, this corresponds to the symmetric resonance.)

### 163 3. Gain threshold and singular frequency

164 In the previous section, we discussed how one can calculate the singular resonance frequency  
 165  $\omega_{sp}$ , using equation 12, as a function of the aspect ratio  $\rho$ . In figure 1, we present the results of  
 166 this calculation for silver (fig. 1a) and gold (fig. 1b). We shall also assume here and for the rest of  
 167 the article that the background material hosting the gain elements in the nanoparticle is silica  
 168 ( $\varepsilon_b = 2.1316$ ) and the external medium is water ( $\varepsilon_h = 1.769$ ).

169 Here one can see that in the core-shell configuration, the singular resonance frequency is  
 170 basically constant (black line): this should be understood because it essentially reflects the  
 171 position of the plasmonic resonance of the metallic core as  $\rho$  is changed, which is well-known  
 172 to be mostly insensitive to size in the quasi-static regime of polarizability we considered. In  
 173 contrast, in the nano-shell configuration (magenta line),  $\omega_{sp}$  redshifts as  $\rho$  increases: this is also  
 174 expected, since this resonance reflects mostly the symmetric mode of the nanoshell [39].

175 It is also worth stressing again that, once the value for  $\rho$  is decided, the singular resonance  
 176 center-line  $\omega_{sp}$  calculated using equation 12, represents the ideal center-line frequency of the  
 177 gain permittivity  $\varepsilon_g(\omega)$  maximizing the plasmon-gain coupling, which could be interesting from  
 178 an experimental standpoint.

179 We have also shown how one can use equation 13 to calculate the minimal amount of gain  
 180  $G_{th}$  (threshold) needed to produce a singular behaviour in the polarizability of core-shells and  
 181 nano-shells. In figure 2 we present the results of this calculation for silver (fig. 2a) and gold  
 182 (fig. 2b), plotting  $G_{th}$  as a function of  $\rho$  in the core-shell (black line) and the nano-shell (magenta  
 183 line) geometries. The first thing one can notice is that in both cases the gain threshold needed  
 184 to produce the singular behaviour is up to an order of magnitude larger for gold than it is for  
 185 silver. This is expected because, compared with silver, gold is a high-loss metal. Also, for both  
 186 metals and for both configurations, the larger the metal volume, hence losses (i. e. larger  $\rho$   
 187 for core-shells and smaller  $\rho$  for nano-shells), the bigger the level of required gain  $G_{th}$  to drive  
 188 emission. (Ripples in the graph for silver come from strong measurement uncertainties in the the  
 189 low-energy range of the Johnson & Christy data [32].)

190 It is important to mention that the results presented in this section (fig. 1 and fig. 2), only  
 191 depend on the radius ratio  $\rho$  and not on the total nanoparticle volume (i. e. ranging  $\rho$  by fixing

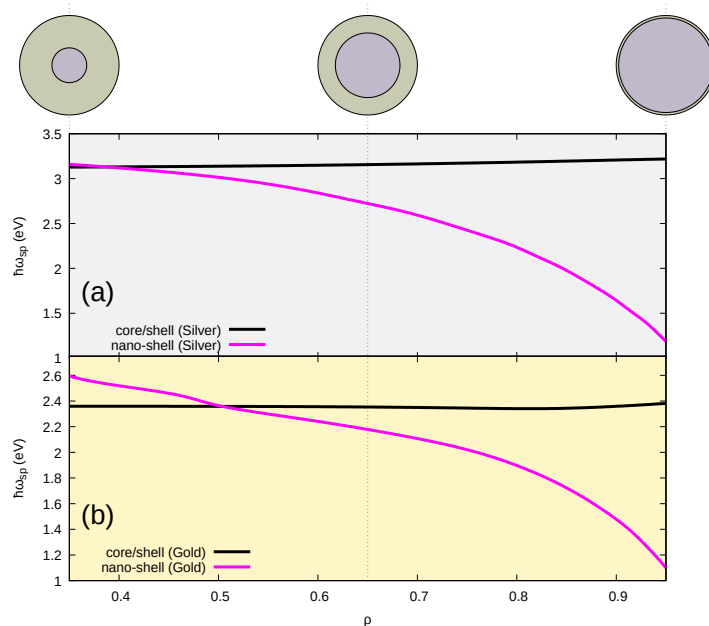


Fig. 1. Singular resonance frequency  $\omega_{sp}$  as a function of the radius ratio  $\rho$ . (a) black: silver core-shell configuration, magenta: silver nano-shell configuration; (b) black: gold core-shell configuration, magenta: gold nano-shell configuration.

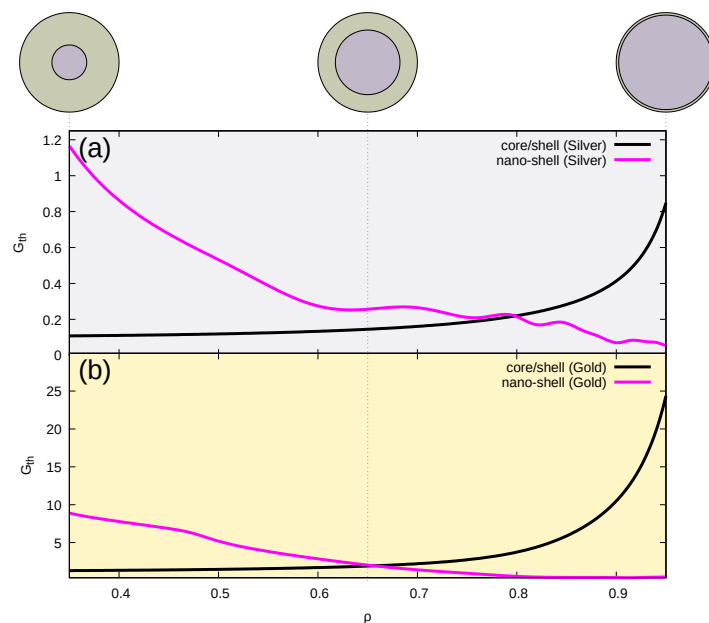


Fig. 2. Gain threshold  $G_{th}$  as a function of the radius ratio  $\rho$ . (a) black: silver core-shell configuration, magenta: silver nano-shell configuration; (b) black: gold core-shell configuration, magenta: gold nano-shell configuration.

192  $r_1$  and changing the shell thickness or fixing  $r_2$  and varying the core volume would produce  
 193 the same results), because again we restrict ourselves to the quasi-static regime of polarization  
 194 only. Obviously, for sizes too big to lie in this regime, one would need to take into account  
 195 the size-dependent dipolar polarizability calculated from the full Mie theory, as well as higher  
 196 multipoles; the same methodology as exploited here could be applied, in principle, to higher-order  
 197 polarizabilities, as long as one stays outside the emissive regime (nanolasing) [37].

198 In the following sections, we will present how the polarizability lineshapes  $\alpha(\omega)$  evolve in  
 199 these structures for different values of  $\rho$  different amounts of gain  $G$ .

#### 200 4. Low-loss metal behavior

201 In figure 3, we present the spectral behavior for a silver core-shell particle with a gain-enriched  
 202 silica shell, and dispersed in water. In the quasi-static regime, the total particle volume intervenes  
 203 as a mere scaling factor in eq. 1, and we therefore plot the real and imaginary parts of the reduced  
 204 polarizability  $\alpha(\omega)/(4\pi r_2^3)$  to dismiss such irrelevant size effects. (Note also that we have chosen  
 a realistic value for the emitter's bandwidth  $\Delta$ :  $\hbar\Delta = 0.15$  eV.)

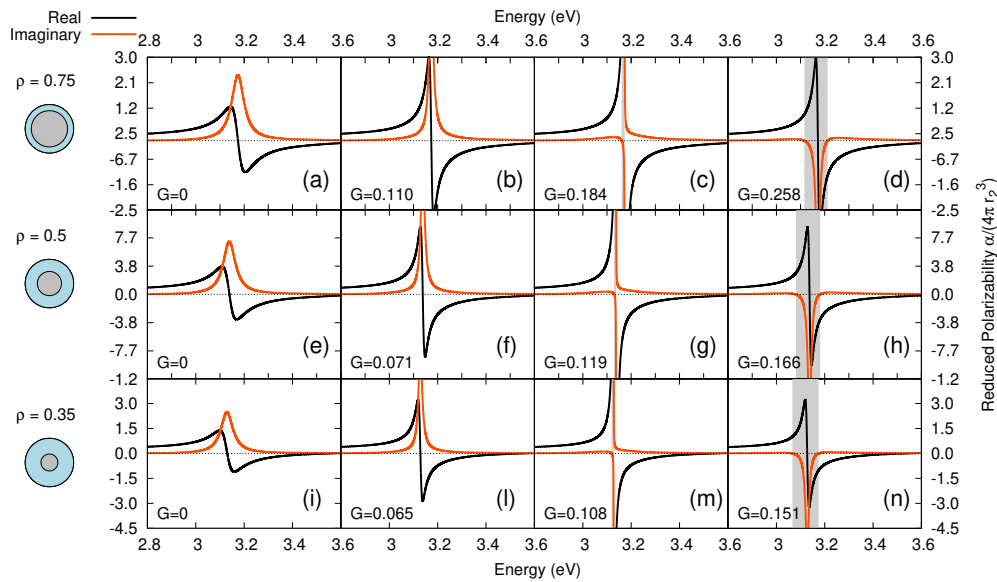


Fig. 3. *Silver core-shell*: Evolution of the plasmon resonance of a 20-nm core-shell nanoparticle embedding a silver-core in a gain-enriched silica shell and dispersed in water. Black curves: real part of the reduced polarizability, orange curves: imaginary part. As gain is increased (from left to right) and for different shell thickness [increasing from up to down] before and after the singular plasmon values [(c), (g), (m)]. Parameters:  $\epsilon_h = 1.769$  (water),  $\epsilon_b = 2.1316$  (silica),  $\omega_g = \omega_{sp}$  and  $\hbar\Delta = 0.15$  eV. The frequency ranges in which the system becomes emissive ( $\alpha''(\omega) < 0$ ) are highlighted in gray.

205

206 The spectra here do not differ much from those found in the case of a single silver particle  
 207 in a uniform gain medium [30]. Specifically, for every row and from left to right one can see a  
 208 plasmon of increasing quality and amplitude as the gain level  $G$  increases from zero (in fig. 3a, e,  
 209 i), until the singular point ( $G = G_{th}$ ) is reached (see fig. 3c, g, m). It is important to emphasize  
 210 here that, for these structures, the imaginary part of the polarizability  $\alpha''(\omega)$  becomes negative  
 211 only for  $G \geq G_{th}$ , meaning that the singular gain  $G_{th}$  indeed represents here the threshold between  
 212 an absorptive and an emissive regime.

213 As  $G$  increases beyond the singular point, the quality of the plasmon resonance gradually  
 214 degrades due to excess gain, but it acquires a growing negative imaginary part (see grey-shaded  
 215 areas in fig. 3d, h, n): as discussed in section 1, this corresponds to a frequency region where our  
 216 simple model breaks down and where a more complete model allowing for a full spatio-temporal  
 217 dynamics has to be used [37,40]. Therefore, all curves in these gray regions, should not be  
 218 taken literally (for this figure and in all subsequent figures presenting a spectrum). Inside the  
 219 grey regions, results in the related geometry studied in [37] strongly suggest that an exponential  
 220 amplification (instability) in the field intensity should occur, yielding appropriate conditions for  
 221 spasing/nanolasing to appear [20,23]. (And this is indeed fully confirmed by our more recent  
 222 work on the specific dynamics of the nano-shell geometry [40]). Therefore, one can consider  
 223 formula 13 as the simplest, existing way to evaluate the minimal amount of gain necessary to  
 224 realize nano-emitters out of these structures.

225 In figure 4, we present the spectral behavior for a silver nano-shell particle embedding a gain  
 enriched silica core and dispersed in water. There are two main advantages here, compared

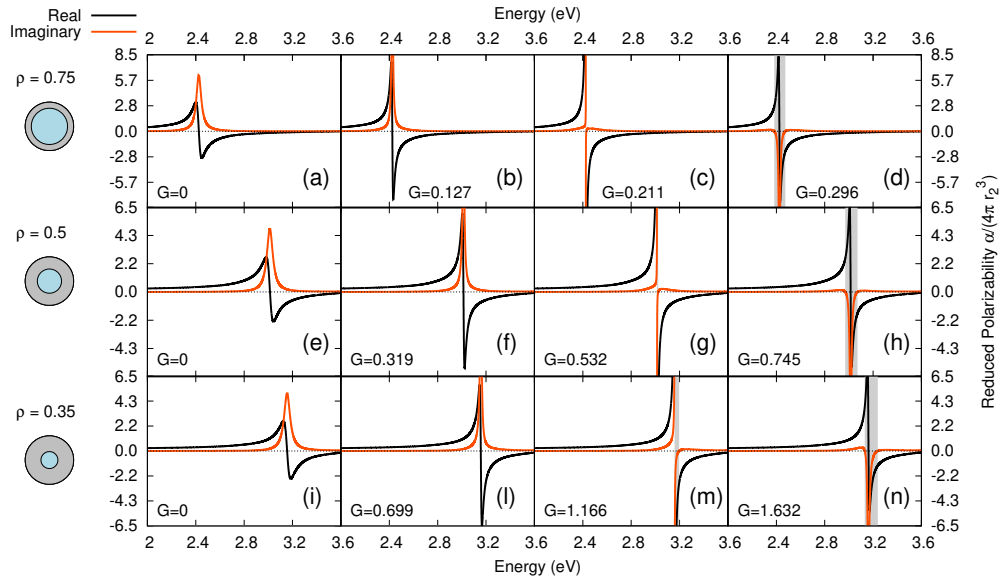


Fig. 4. *Silver nano-shell*: Evolution of the plasmon resonance of a 20-nm nano-shell particle embedding a gain enriched silica core in a silver shell and diluted in water. As gain is increased (from left to right) and for different shell thickness [increasing from up to down] before and after the singular plasmon values [(c), (g), (m)]. Parameters:  $\epsilon_h = 1.769$  (water),  $\epsilon_b = 2.1316$  (silica),  $\omega_g = \omega_{sp}$  and  $\hbar\Delta = 0.15$  eV. The frequency ranges in which the system becomes emissive ( $\alpha''(\omega) < 0$ ) are highlighted in gray.

226 with the previous core-shell case. First, as observed in fig. 1, the singular frequency changes  
 227 significantly as  $\rho$  is varied, as is usual with nanoshells. This could allow for some flexibility to  
 228 position the singular resonance frequency  $\omega_{sp}$  on the fixed emission center frequency  $\omega_g$  of any  
 229 predetermined gain medium, which may prove easier in practice than to find a dye emitting as  
 230 close as possible to the fixed singular resonance in the case of core-shells. Another advantage of  
 231 the nanoshell configuration is that the field inside the core keeps uniform, and the plasmonic field  
 232 outside the particle keeps dipolar, even in the emissive regimes (grey regions in fig. 4c, g, m, d, h,  
 233 n), leading to single-mode nanolasing. On the contrary, core-shell systems will suffer a “mode  
 234 cascade mechanism” which will inevitably lead to multi-mode lasing, as was discussed in [37].  
 235

236 **5. High-loss metal behavior**

237 As in the case of a single particle in a uniform medium [30], the spectral response of a gold core-shell nanoparticle appears to be richer than its silver counterpart. The first thing one can

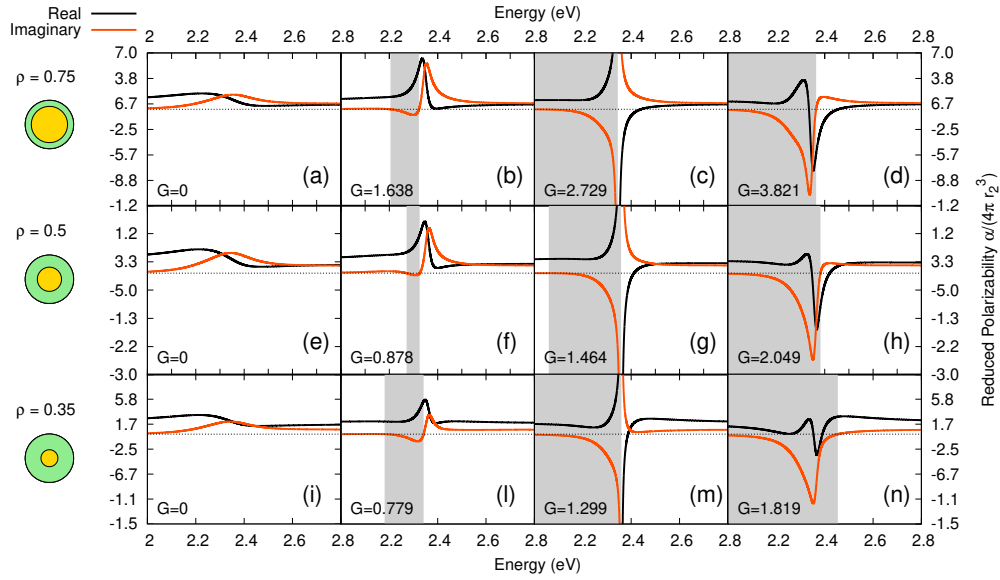


Fig. 5. *Gold core-shell*: Evolution of the plasmon resonance of a 20-nm core-shell nanoparticle embedding a gold-core in a gain enriched silica-shell and dispersed in water. Black curves: real part of the reduced polarizability, orange curves: imaginary part. As gain is increased (from left to right) and for different shell thickness [increasing from up to down] before and after the singular plasmon values [(c), (g), (m)]. Parameters:  $\epsilon_h = 1.769$  (water),  $\epsilon_b = 2.1316$  (silica),  $\omega_g = \omega_{sp}$  and  $\hbar\Delta = 0.15$  eV. The frequency ranges in which the system becomes emissive ( $\alpha''(\omega) < 0$ ) are highlighted in gray.

238 notice in figure 5 is that, due to the higher metal losses, the gain threshold  $G_{th}$  necessary to  
 239 produce the singular behavior (fig. 5c, g, m) is around twenty times larger than the one for silver  
 240 (fig. 3c, g, m), again showing gold a less promising candidate for nanolasing applications than  
 241 silver. Also, for the same reason, the plasmon resonance in absence of gain (fig. 5a, e, i) is less  
 242 pronounced compared to that of silver and also much more distorted as an effect of the interband  
 243 transitions.  
 244

245 The most interesting aspect here is that, the high level of gain necessary to drive any response,  
 246 produces an additional deformation on the plasmonic resonance even before the singular point  
 247 (fig. 5b, f, l). When a thick shell is considered and an amount of gain lower than the one needed to  
 248 drive the singular behavior is added to the system ( $G < G_{th}$ ) as in fig. 5l), we observe a *real*  
 249 part of the polarizability  $\alpha'(\omega)$  having a bell-like shape (whereas this is usually seen for imaginary  
 250 response), and conversely, the *imaginary* part  $\alpha''(\omega)$  has here the sigmoidal shape normally  
 251 expected for real part. Similar shapes are observed for thicker shells (not shown). This behavior,  
 252 called “conjugate plasmon” is due to Fano-type resonances, and was theoretically predicted for  
 253 the first time in the case of a metal particle in a uniform gain medium [30]. Conjugate plasmons  
 254 show one particularly attractive property: at the plasmon frequency, where the real response is  
 255 maximal, losses are also close to zero; which is in fact much more favorable for most of practical  
 256 applications than the situation of usual plasmons.

257 When thinner shells are considered, the deformed spectral response does not produce an  
 258 actual swap between the real and the imaginary part of  $\alpha(\omega)$ , instead, these appear to be quite

259 symmetrical, still keeping the interesting propriety of having a large, positive real part where  
 260 the losses are negligible. Moreover, when thin shells are considered and an amount of gain  
 261 greater than  $G_{th}$  is used (fig. 5d, h), an even more interesting symmetrical situation appears:  
 262 while the conjugate plasmons obtained before the singular point have a positive real part, here  
 263 they display a negative real part. This type of responses where the real part of  $\alpha$  is significant  
 264 and the imaginary part is negligible, could be extremely valuable, if one is interested in obtaining  
 265 artificial, low-loss media with so-called “negative” properties. The important setback here is  
 266 that this is observed for very high (probably unrealistic) gain levels in the system, and also these  
 267 features lies very close to the emissive spectral region (grey regions in fig. 5b, f, l, d, h), which  
 268 could limit the possibility to use this propriety for applications.

269 Finally, quite interestingly, it should be stressed that due to the strong spectral deformations  
 270 related to high losses and interband transitions, the system becomes emissive for amounts of  
 271 gain *less* than the threshold gain needed to produce the singular behavior (see the grey regions in  
 272 fig. 5b, f, l). The exact nature of these “low-gain” emissive states as compared to those obtained  
 273 for ( $G < G_{th}$ ) remains to be explored, but paradoxically enough, this indicates that the interband  
 274 transitions may provide ways to reduce emission with lower gain levels than expected for gold.

275 We conclude the study of plasmon spectra with figure 6, where the spectral behavior of gold  
 nano-shell structures is presented. Here one can easily see that particles with thin gold shells

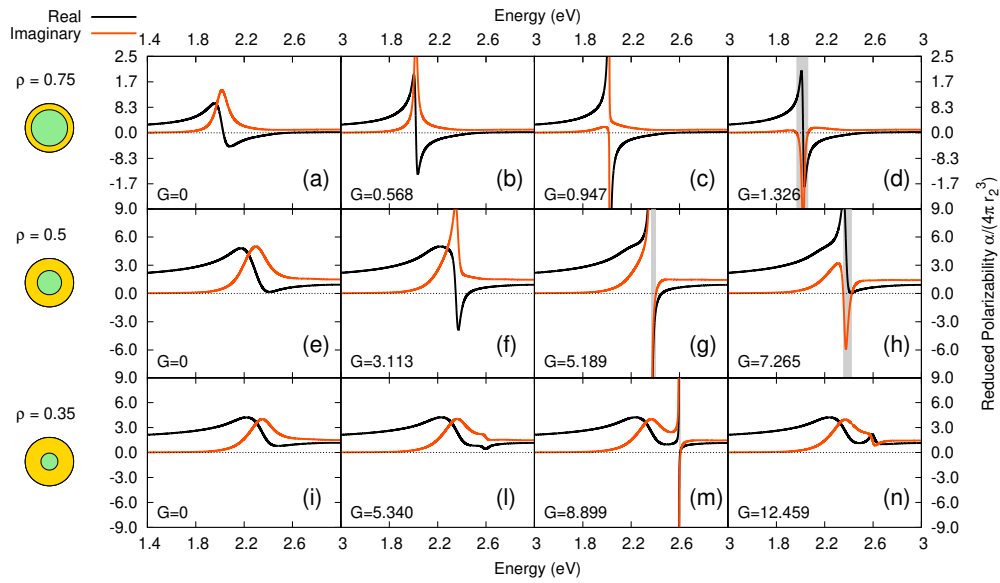


Fig. 6. *Gold nano-shell*: Evolution of the plasmon resonance of a 20-nm nano-shell nanoparticle embedding a gain enriched silica core in a gold shell and dispersed in water. Black curves: real part of the reduced polarizability, orange curves: imaginary part. As gain is increased (from left to right) and for different shell thickness [increasing from up to down] before and after the singular plasmon values [(c), (g), (m)]. Parameters:  $\epsilon_h = 1.769$  (water),  $\epsilon_b = 2.1316$  (silica),  $\omega_g = \omega_{sp}$  and  $\hbar\Delta = 0.15$  eV. The frequency ranges in which the system becomes emissive ( $\alpha''(\omega) < 0$ ) are highlighted in gray.

276  
 277 behave basically the same as silver nanoshells (fig. 6a-d). Provided that enough gain is included  
 278 in the system, the same spectral behavior appears until around  $\rho \sim 0.5$ . However, as soon as  
 279 the metal volume fraction increases more, the extremely high level of gain necessary to drive  
 280 any enhancement in the resonance, produces an additional deformation in the spectra (fig. 6e-n),  
 281 up to the point where the losses are so high that, even if we still observe a singular behavior

282 (fig. 6m), any emission seems to be lost for larger quantities of gain (fig. 6n). In such situations  
 283 where extreme gain competes with extreme losses, other physical effects (not included in this  
 284 model) may rise; for this reason, we would definitely suggest caution in acquiring the spectral  
 285 results presented in figs. 6i-n.

## 286 6. Density of gain elements (emitters)

287 It is of prime importance, for the reasons mentioned in the last paragraph and others, to provide  
 288 a way to quantitatively evaluate if a gain level is realistically attainable or not. For this reason  
 289 one has to relate the  $G$  parameter of equation 2 with real physical quantities. There are different  
 290 approaches to do this: here we solve the time dynamical model for gain elements based on the  
 291 optical Bloch equations we presented in a previous work [37], looking for the steady state regime.  
 292 The result of this calculation gives:

$$\varepsilon_g = \varepsilon_b + \frac{2n\mu^2 N}{3\hbar\varepsilon_0[2(\omega - \omega_g) + i\Delta]} \quad (14)$$

We remind the reader that  $n$  is the volume density of gain elements (emitters such as dye molecules, quantum dots, etc.),  $\mu$  the transition dipole moment of the emitters,  $N$  is the population inversion (i. e. the pumped fraction of the of the gain elements population) and  $\hbar$  the reduced Plank constant. Comparing equation 14 with equation 2, we get the equation 3 presented in the beginning of this article, that is:

$$G = \frac{2n\mu^2}{3\hbar\varepsilon_0\Delta} \tilde{N}.$$

293 From the latter, one can calculate the volume density  $n$  of emitters:

$$n = \frac{3\hbar\varepsilon_0\Delta}{2\mu^2 N} G, \quad (15)$$

294 which gives a relation between the gain level  $G$  in the system and the required emitter density  
 295  $n$  to generate it. It also allows to calculate the emitter density  $n_{\text{th}}$  necessary to reach the lasing  
 296 threshold  $G = G_{\text{th}}$  and produce a singular resonance as:

$$n_{\text{th}}(\rho) = \frac{3\hbar\varepsilon_0\Delta}{2\mu^2 N} G_{\text{th}}(\rho), \quad (16)$$

297 It is worth recalling that, as discussed previously, in order for  $G_{\text{th}}$  (and thus for  $n_{\text{th}}$ ) to be only  
 298 function of  $\rho$ , one has to align the gain element center-line emission with the plasmon resonance  
 299 ( $\omega_g = \omega_{\text{sp}}$ ); moreover if we consider a fully pumped nanoparticle ( $\tilde{N} = 1$ ), all of the constants in  
 300 equation 16 are already set but the transition dipole moment  $\mu$ . In the following characterization,  
 301 we plot  $n_{\text{th}}$  as a function of the aspect ratio  $\rho$ , considering dyes with transition dipole moments in  
 302 the range  $\mu = 10 \pm 5$  D, comparable to the classical dye Rhodamine 123 ( $\mu_R \sim 8.1$  D) [41].

303 The results of this characterization are presented in figure 7 for core-shell and in figure 8 for  
 304 nano-shell structures. In both figures, the continuous lines (resp. black line for silver, and orange  
 305 line for gold) are calculated for  $\mu = 10D$ , while the shaded areas (resp. yellow for gold and  
 306 grey for silver) show how  $n_{\text{th}}$  changes by varying  $\mu$  in the interval  $5 \text{ D} \leq \mu \leq 15 \text{ D}$  (the lowest  
 307 border corresponds to the highest  $\mu$ ). For reference, we also compared the found densities with  
 308 the density of the close-packing of spheres in a dense arrangement [42],  $n_{\text{CP}} = 0.74$ : this is  
 309 materialized by a red horizontal line, above which emitters density are geometrically prohibited.  
 310 This should be understood as a mere indication of maximum densities, since the gain medium  
 311 is expected to structurally collapse well before the geometrical limit, as the host matrix (e.g.,  
 312 silica) is gradually replaced by emitters. Also, at high densities, even before two gain elements

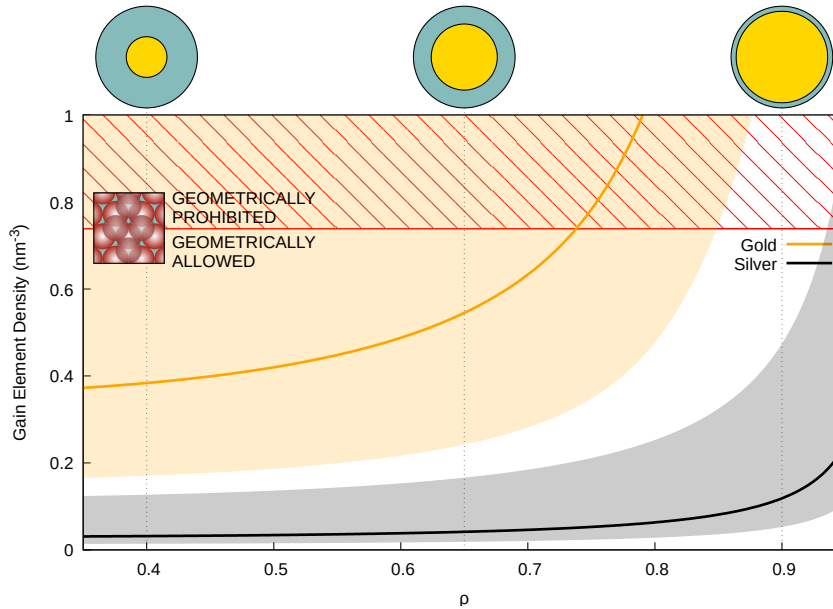


Fig. 7. Threshold emitter density  $n_{\text{th}}$  as a function of the aspect ratio  $\rho$  for a core-shell structure. *orange line*: Gold core. The continuous line refers to  $\mu = 10$  D, the yellow shaded area to the interval  $5 \text{ D} \leq \mu \leq 15 \text{ D}$  (see main text). *Black line*: Silver core. The continuous line refers to  $\mu = 10$  D, the grey shaded area to the interval  $5 \text{ D} \leq \mu \leq 15 \text{ D}$  (see main text). The horizontal red line corresponds to the dense packing limit for spheres.

313 physically touch each other, emitter-emitter couplings can become strongly detrimental for their  
 314 efficiency [43–46].

315 The first thing one can appreciate in figure 7 is that, no matter if using a gain element with  
 316 transition dipole moment as low as  $\mu = 5$  D it is still possible to fit enough elements to drive a  
 317 singular behavior up to very thin shells. On the other hand, when gold is used, due to stronger  
 318 metallic losses, low transition dipole moments do not allow singular behavior with realistic  
 319 emitter densities; even with  $\mu = 10$  D, it is necessary to have enough gain, i.e. thick enough  
 320 shells, to allow for it ( $\rho \lesssim 0.65$ ).

321 In figure 8 we present the same characterization for nano-shell particles. Here one has to  
 322 consider that the higher metal volume fraction is for thick shells (low  $\rho$ ) and consequently, the  
 323 particle density needed to produce the singular behavior gets lower for higher  $\rho$  (thin shells). One  
 324 can observe ripples, which are again due to measurements discrepancies in the low-energy end of  
 325 the silver permittivity data we used [32]. If one compares the behavior for a silver nano-shell  
 326 (fig. 8: black continuous line) with the one of a nano-shell made of gold (fig. 8: orange continuous  
 327 line), it is evident once again that, due to the lower losses in silver, it is possible to use a wider  
 328 range of shell thicknesses and still be able to fit enough gain in the core to produce a singular  
 329 behavior: even with a gain element with a relatively low transition dipole moment one can,  
 330 in principle, still obtain emission with thick-shell-particles ( $\rho \sim 0.5$ ). Also, when using gain  
 331 elements with a transition dipole moment of around 10 D it appears to be possible to realize an  
 332 emissive silver nano-shell up to very thick shells ( $\rho \lesssim 0.3$ ).

333 Finally, we can confirm here what we anticipated when discussing fig. 6: it appears to be  
 334 impossible to fit enough gain in the core of a gold nano-shell particle with a thick shell ( $\rho \lesssim 0.5$ ),  
 335 even when using high transition dipole moment ( $\mu \sim 15$  D) gain elements. This means that,

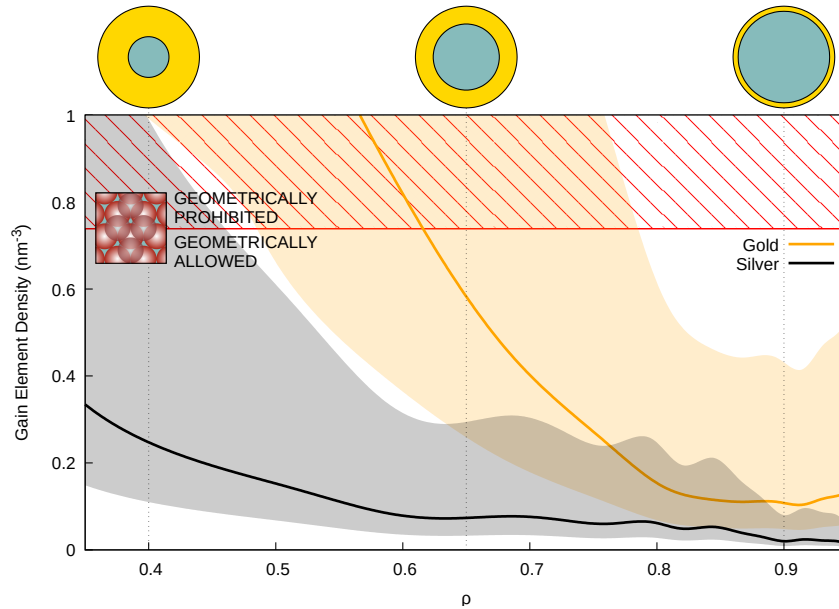


Fig. 8. Threshold emitter density  $n_{th}$  as a function of the aspect ratio  $\rho$  for a nano-shell structure. *Orange line*: Gold shell. The continuous line refers to  $\mu = 10 D$ , the yellow shaded area to the interval  $5 D \leq \mu \leq 15 D$  (see main text). *Black line*: Silver shell. The continuous line refers to  $\mu = 10 D$ , the grey shaded area to the interval  $5 D \leq \mu \leq 15 D$  (see main text). The horizontal red line corresponds to the dense packing limit for spheres.

336 unless a new gain element with an extraordinary transition dipole moment is developed, the  
 337 spectra presented in figure 6e-n for gold are not realistically realizable.

338 Summarizing, when silver is used, it appears that both the core-shell and the nano-shell are  
 339 viable candidates to realize a plasmonic emitter; when gold is used, nano-shells are a better  
 340 solution unless very-high-transition-dipole gain elements are employed. Finally, in the pursuit for  
 341 the ideal gain element, size is a hidden factor that might not be evident in our characterization:  
 342 the gain element radius is in fact relevant because, as an example, high transition dipole moment  
 343 quantum dots tend to have typical diameter ranging between 2 and 10 nm [47, 48], and may be  
 344 too big to reach high packing densities, or to even fit in small nanoparticles (like the ones we  
 345 focused on), requiring large, multipolar ones instead.

## 346 7. Designing a gain-assisted nanoparticle for singular resonance

347 We will now harvest from our characterization a step by step procedure to facilitate the design of  
 348 a gain assisted nanoparticle including enough gain to allow a singular resonance.

- 349 • Firstly one can use equation 12 to calculate the singular plasmon frequency when  $\omega_g = \omega_{sp}$   
 350 or (and this is especially effective for nano-shells) set the desired singular frequency  $\omega_{sp}$   
 351 and use the same equation to determine the right radius ratio  $\rho$ ;
- 352 • once  $\omega_{sp}$  is set, one has to look for a gain element whose emission central frequency is the  
 353 closest possible to it ( $\omega_g \sim \omega_{sp}$ ) to maximize the coupling efficiency;
- 354 • if the found gain emission frequency is different from the singular plasmon frequency  
 355 ( $\omega_g \neq \omega_{sp}$ ), one can use equation 10 to calculate the new singular frequency and equation 11

356 to calculate the threshold gain  $G_{th}$ , else (if  $\omega_g = \omega_{sp}$ ) one can directly use equation 13 to  
357 calculate  $G_{th}$ ;

- 358 • knowing  $G_{th}$ , one can use equation 16 to calculate the threshold particle density to be  
359 included in the shell (core-shells) or in the core (nano-shells) to allow for a singular  
360 resonance when completely pumped.

361 It is of prime importance to stress here that, at this stage, the presented procedure is not meant to  
362 be taken as a recipe or as a validated protocol, but more as an indication of the most promising  
363 direction to be explored in order to experimentally test our findings.

## 364 8. Conclusions

365 We have studied the plasmonic response of metal nanoparticles in the core-shell and nano-shell  
366 configurations, when pumped gain elements are added to the system. The findings of this simple,  
367 steady state approach can be validated using a more complex, dynamical, multipolar model (as  
368 the one we presented in a previous work [37]) until the gain threshold needed to overcompensate  
369 the metal losses and driven emission is reached.

370 Taking advantage of the simplicity of this model, we generalized a method allowing to calculate  
371 both the threshold gain  $G_{th}$  and the singular resonance frequency  $\omega_{sp}$  (nanolasing frequency)  
372 for both core-shell and nano-shell particles. When the efficiency of the coupling between the  
373 gain elements and the plasmon is maximized (by superimposing the gain emission line with the  
374 plasmonic resonance  $\omega_g = \omega_{sp}$ ), both the singular resonance frequency and the threshold gain  
375 are only function of  $\rho$ . We used this simplified dependency to characterize the evolution of the  
376 plasmonic spectral shape as a function of the gain added for both core-shells and nano-shells  
377 made in gold and silver, we discussed up to what point these spectra are reliable, where and when  
378 this model breaks and what one can expect when it does.

379 This way we have shown that the quality of the resonances can be drastically enhanced until  
380 the response can become singular at  $G_{th}$ , this is especially true for metals with a low level of  
381 losses like silver, where additional gain only produces an increasing quality of the plasmon  
382 resonance towards the singular point, without introducing any additional deformation in the  
383 spectral shape. In gold, due to the higher loss associated with the interband transition, the  
384 situation is richer. Deformed spectra as the “conjugate” plasmon appear revealing spectral  
385 responses that, if realizable, could be harbingers of novel applications.

386 We discussed that, when the imaginary part of the polarizability gets negative, one can expect  
387 emission in that frequency range; and also mentioned that, when this happens, a quantitative  
388 description of the phenomenon falls out of the scope of our model.

389 Finally we proposed a way to determine if a gain level  $G$  is realistic or not, by translating it in  
390 terms of particle density  $n$  and comparing this last to the close-packing of equal spheres is a dense  
391 arrangement, this way we have shown that depending on the transition dipole moment  $\mu$  of the  
392 used gain, some configuration are more realistic than others and, as expected, silver nanoparticles  
393 sporting the lowest possible metal volume-ratio are better candidates for the realization of an  
394 emitting plasmonic nanoparticle. Eventually, we reorganized all of our findings in a step by step  
395 procedure aimed to facilitate the synthesis of nanoparticles which could potentially being driven  
396 to emission.

397 The presented model is general and it can be easily customized to describe a wider range  
398 of different materials and configuration. Fine tuning, using different particle sizes and gain  
399 elements, can easily be done allowing the possibility to design different nanostructures optimized  
400 for diverse cutting edge optical applications.

## 401 9. Disclosures

402 The authors declare no conflicts of interest.

## 403 10. Data availability

404 Data underlying the results presented in this paper are not publicly available at this time but may  
405 be obtained from the authors upon reasonable request.

## 406 References

- 407 1. S. A. Ramakrishna and J. B. Pendry, "Removal of absorption and increase in resolution in a near-field lens via optical  
408 gain," *Phys. Rev. B* **67**, 201101.1–201101.4 (2003).
- 409 2. N. M. Lawandy, "Localized Surface Plasmon Singularities in Amplifying Media," *Appl. Phys. Lett.* **85**, 5040–5042  
410 (2004).
- 411 3. M. A. Noginov, G. Zhu, M. Bahoura, J. Adegoke, C. E. Small, B. A. Ritzo, V. P. Drachev, and V. M. Shalaev,  
412 "Enhancement of surface plasmons in an Ag aggregate by optical gain in a dielectric medium," *Opt. Lett.* **31**,  
413 3022–3024 (2006).
- 414 4. M. Wegener, J. García-Pomar, C. Soukoulis, N. Meinzer, M. Ruther, and S. Linden, "Toy model for plasmonic  
415 metamaterial resonances coupled to two-level system gain," Arxiv preprint arXiv:0809.0487 (2008).
- 416 5. A. Fang, T. Koschny, and C. Soukoulis, "Self-consistent calculations of loss-compensated fishnet metamaterials,"  
417 *Phys. Rev. B* **82**, 121102 (2010).
- 418 6. S. Xiao, V. Drachev, A. Kildishev, X. Ni, U. Chettiar, H. Yuan, and V. Shalaev, "Loss-free and active optical  
419 negative-index metamaterials," *Nature* **466**, 735–738 (2010).
- 420 7. A. Chipouline, J. Petschulat, A. Tuennermann, T. Pertsch, C. Menzel, C. Rockstuhl, F. Lederer, and V. A. Fedotov,  
421 "Multipole model for metamaterials with gain: from nano-laser to quantum metamaterials," in *Metamaterials VI*, vol.  
422 8070 V. Kuzmiak, P. Markos, and T. Szoplik, eds., International Society for Optics and Photonics (SPIE, 2011), pp.  
423 123 – 131.
- 424 8. S. Liu, J. Li, F. Zhou, L. Gan, and Z. Li, "Efficient surface plasmon amplification from gain-assisted gold nanorods,"  
425 *Opt. letters* **36**, 1296–1298 (2011).
- 426 9. S. Wuestner, A. Pusch, K. Tsakmakidis, J. Hamm, and O. Hess, "Overcoming losses with gain in a negative refractive  
427 index metamaterial," *Phys. review letters* **105**, 127401 (2010).
- 428 10. P. Bolger, W. Dickson, A. Krasavin, L. Liebscher, S. Hickey, D. Skryabin, and A. Zayats, "Amplified spontaneous  
429 emission of surface plasmon polaritons and limitations on the increase of their propagation length," *Opt. letters* **35**,  
430 1197–1199 (2010).
- 431 11. N. Meinzer, M. Ruther, S. Linden, C. Soukoulis, G. Khitrova, J. Hendrickson, J. Olitsky, H. Gibbs, and M. Wegener,  
432 "Arrays of Ag split-ring resonators coupled to InGaAs single-quantum-well gain," Arxiv preprint arXiv:1009.0693  
433 (2010).
- 434 12. A. Sarychev and G. Tartakovsky, "Magnetic plasmonic metamaterials in actively pumped host medium and plasmonic  
435 nanolaser," *Phys. Rev. B* **75**, 085436 (2007).
- 436 13. R. F. Oulton, V. J. Sorger, T. Zentgraf, R. Ma, C. Gladden, L. Dai, G. Bartal, and X. Zhang, "Plasmon lasers at deep  
437 subwavelength scale," *Nature* **461**, 629–632 (2009).
- 438 14. J. Zhou, T. Koschny, and C. M. Soukoulis, "An efficient way to reduce losses of left-handed metamaterials." *Opt.*  
439 *Express* **16**, 11147–52 (2008).
- 440 15. G. Strangi, A. De Luca, S. Ravaine, M. Ferrie, and R. Bartolino, "Gain induced optical transparency in metamaterials,"  
441 *Appl. Phys. Lett.* **98**, 251912 (2011).
- 442 16. A. De Luca, M. P. Grzelczak, I. Pastoriza-Santos, L. M. Liz-Marzán, M. L. Deda, M. Striccoli, and G. Strangi,  
443 "Dispersed and Encapsulated Gain Medium in Plasmonic Nanoparticles: a Multipronged Approach to Mitigate  
444 Optical Losses," *ACS Nano* **5**, 5823–5829 (2011).
- 445 17. D. Schurig, J. J. Mock, B. J. Justice, S. A. Cummer, J. B. P. ans A. F. Starr, and D. R. Smith, "Metamaterial  
446 Electromagnetic Cloak at Microwave Frequencies," *Science* **314**, 977–980 (2006).
- 447 18. W. Cai, U. K. Chettiar, A. V. Kildishev, and V. M. Shalaev, "Optical Cloaking with Metamaterials," *Nat. Photon.* **1**,  
448 224–227 (2008).
- 449 19. A. Veltri, "Designs for electromagnetic cloaking a three-dimensional arbitrary shaped star-domain." *Opt. express* **17**,  
450 20494–501 (2009).
- 451 20. M. A. Noginov, G. Zhu, A. M. Belgrave, R. Bakker, V. M. Shalaev, E. E. Narimanov, S. Stout, E. Herz, T. Suteewong,  
452 and U. Wiesner, "Demonstration of a spaser-based nanolaser," *Nature* **460**, 1110–1112 (2009).
- 453 21. E. Plum, V. Fedotov, P. Kuo, D. Tsai, and N. Zheludev, "Towards the lasing spaser: controlling metamaterial optical  
454 response with semiconductor quantum dots," *Opt. Express* **17**, 8548–8550 (2009).
- 455 22. N. Zheludev, S. Prosvirnin, N. Papasimakis, and V. Fedotov, "Lasing Spaser," *Nat. Photon.* **2**, 351–354 (2008).
- 456 23. M. I. Stockman, "Spasers explained," *Nat. Photonics* **2**, 327–329 (2008).
- 457 24. C. Graf and A. van Blaaderen, "Metallo-dielectric Colloidal Core-Shell Particles for Photonic Applications," *Langmuir*  
458 **18**, 524–534 (2002).
- 459 25. O. G. Tovmachenko, C. Graf, D. J. van den Heuvel, A. van Blaaderen, and H. C. Gerritsen, "Fluorescence Enhancement  
460 by Metal-Core/Silica-Shell Nanoparticles," *Adv. Mat.* **18**, 91–95 (2006).
- 461 26. X. Meng, K. Fujita, S. Murai, T. Matoba, and K. Tanaka, "Plasmonically Controlled Lasing Resonance with  
462 Metallic-Dielectric Core-Shell Nanoparticles," *NanoLett.* **11**, 1374–1378 (2011).

- 463 27. A. De Luca, M. Ferrie, S. Ravaine, M. La Deda, M. Infusino, A. Rashed, A. Veltri, A. Aradian, N. Scaramuzza, and  
464 G. Strangi, "Gain functionalized core-shell nanoparticles: the way to selectively compensate absorptive losses," *J.*  
465 *Mater. Chem.* (2012).
- 466 28. V. Ponsinet, A. Aradian, P. Barois, and S. Ravaine, "Self-Assembly and Nanochemistry Techniques for the Fabrication  
467 of Metamaterials," in *Metamaterials Handbook vol.2: Applications of Metamaterials*, F. Capolino, ed. (CRC Press,  
468 2009), pp. 32–1 – 32–39.
- 469 29. A. Aradian, P. Barois, O. Mondain-Monval, V. Ponsinet, and A. Baron, "The Bottom-Up Approach toward Artificial  
470 Optical Magnetism in Metastructures," in *Hybrid Flatland Metastructures*, R. Caputo and G. E. Lio, eds. (AIP  
471 Publishing, 2021), pp. 3–1 – 3–28.
- 472 30. A. Veltri and A. Aradian, "Optical response of a metallic nanoparticle immersed in a medium with optical gain,"  
473 *Phys. Rev. B* **85**, 115429 (2012).
- 474 31. J. D. Jackson, *Classical Electrodynamics* (Wiley, New York, 1998), 3rd ed.
- 475 32. P. B. Johnson and R. W. Christy, "Optical Constants of the Noble Metals," *Phys. Rev. B* **6**, 4370–4379 (1972).
- 476 33. V. Caligiuri, L. Pezzi, A. Veltri, and A. De Luca, "Resonant Gain Singularities in 1D and 3D Metal/Dielectric  
477 Multilayered Nanostructures," *ACS Nano* **11**, 1012–1025 (2017).
- 478 34. M. Infusino, A. De Luca, A. Veltri, C. Vázquez-Vázquez, M. Correa-Duarte, R. Dhama, and G. Strangi, "Loss-  
479 Mitigated Collective Resonances in Gain-Assisted Plasmonic Mesocapsules," *ACS Photonics* **1**, 371–376 (2014).
- 480 35. P. Polimeno, F. Patti, M. Infusino, J. J. Sanchez, M. A. Iati, R. Saija, G. Volpe, O. M. Marago, and A. Veltri, "Gain-  
481 Assisted Optomechanical Position Locking of Metal/Dielectric Nanoshells in Optical Potentials," *ACS Photonics*  
482 (2020).
- 483 36. P. Polimeno, F. Patti, M. Infusino, M. A. Iati, R. Saija, G. Volpe, O. M. Maragò, and A. Veltri, "Optical trapping of  
484 gain-assisted plasmonic nano-shells: theoretical study of the optical forces in a pumped regime below the emission  
485 threshold," in *Optical Trapping and Optical Micromanipulation XVIII*, vol. 11798 K. Dholakia and G. C. Spalding,  
486 eds., International Society for Optics and Photonics (SPIE, 2021), pp. 170 – 177.
- 487 37. A. Veltri, A. Chipouline, and A. Aradian, "Multipolar, time-dynamical model for the loss compensation and lasing of  
488 a spherical plasmonic nanoparticle spaser immersed in an active gain medium," *Sci. Reports* **6**, 33018 (2016).
- 489 38. D. Baranov, E. Andrianov, A. Vinogradov, and A. Lisyansky, "Exactly solvable toy model for surface plasmon  
490 amplification by stimulated emission of radiation," *Opt. express* **21**, 10779–91 (2013).
- 491 39. E. Prodan and P. Nordlander, "Structural tunability of the plasmon resonances in metallic nanoshells," *Nano Lett.* **3**,  
492 543–547 (2003).
- 493 40. A. Veltri, A. Aradian *et al.*, to be published .
- 494 41. P.-H. Chung, C. Tregidgo, and K. Suhling, "Determining a fluorophore's transition dipole moment from fluorescence  
495 lifetime measurements in solvents of varying refractive index," *Methods Appl. Fluoresc.* **4**, 045001 (2016).
- 496 42. Wikipedia contributors, "Close-packing of equal spheres — Wikipedia, the free encyclopedia," (2021). [Online;  
497 accessed 20-July-2021].
- 498 43. P. Andrew and W. L. Barnes, "Forster energy transfer in an optical microcavity," *Science* **290**, 785–788 (2000).
- 499 44. J. Zhang, Y. Fu, M. H. Chowdhury, and J. R. Lakowicz, "Enhanced Forster Resonance Energy Transfer on Single  
500 Metal Particle," *J. Chem. Phys.* **111**, 50–56 (2007).
- 501 45. X. Zhang, C. A. Marocico, M. Lunz, V. A. Gerard, Y. K. Gun'Ko, V. Lesnyak, N. Gaponik, A. S. Susha, A. L.  
502 Rogach, and A. L. Bradley, "Experimental and theoretical investigation of the distance dependence of localized  
503 surface plasmon coupled forster resonance energy transfer," *ACS Nano* **8**, 1273–1283 (2014).
- 504 46. P. Ghenuche, M. Mivelle, J. De Torres, S. B. Moparthi, H. Rigneault, N. F. Van Hulst, M. F. García-Parajó, and  
505 J. Wenger, "Matching Nanoantenna Field Confinement to FRET Distances Enhances Förster Energy Transfer Rates,"  
506 *Nano Lett.* **15**, 6193–6201 (2015).
- 507 47. S. I. Pokutnyi, Y. N. Kulchin, and V. P. Dzyuba, "Optical absorption of one-particle electron states in quasi-zero-  
508 dimensional nanogeterostructures: Theory," *Pac. Sci. Rev. A: Nat. Sci. Eng.* **18**, 261–265 (2016).
- 509 48. Wikipedia contributors, "Close-packing of equal spheres — Wikipedia, the free encyclopedia," (2021). [Online;  
510 accessed 23-July-2021].